9

Passive Ranging Based on IR Radiation Characteristics

Yang De-gui and Li Xiang
Institute of Space Electronic Information Technology
College of Electric Science and Engineering, NUDT
China

1. Introduction

Using passive detecting system to range and track target is quite an important researching field in photoelectrical signal processing, and IRST (IR searching and detecting system) is such a system, thus applying which to ranging IR target is a study hotspot all the while.

In recent years, many researchers have made a lot of works and achieved remarkable results. The system effect distance is deduced from different aspects in [1, 2]. Target range is obtained based on the target movement model in [3]. [4] studies the passive ranging of ground target in mono-static and single band condition based on radiance difference between target and background. Ranging expressions are deduced and ranging error is analyzed in [5-7] based on radiance difference, ranging radiate power ratio, target contrast ratio and SNR etc. in condition of mono-static and two bands.

However, above works were not aimed at the staring IR imaging system, that there is no relationship between ranging and IR images though [8-9] deduce the effect distance of the staring IR detection system with no ranging results. Based on these works, starting with the introduction of the staring IR detection system, this paper deduces the ranging expression for point and surface targets based on signal band IR image. The real IR image data validates this method and the ranging error is analyzed.

2. Working principle of the staring IRST

With the development of IR technology, more and more IR caloric imaging systems are adopted by IRST. The caloric imaging system has developed two generations, the first is based on optical and mechanical scanning, and the second is mainly based on staring or scanning focal plane array.

Fig.1 presents the second generation of IRST, which is commonly consisted by optic system, focal surface detecting subassembly, and video signal processing and vision system, there into focal plane array [10] can greatly prompt the scanning velocity and imaging quality. Generally, target detection is not only related with the scene contrast ratio, but also the resolving and analyzing abilities of the detection system. As Fig.1 shows, that the IR radiate

power of the target and its background arrive at the caloric imaging system can be called the first stage of IRST; the power arrives at the focal plane detector with attenuation, then the power signal is changed into signal voltage according to different waveband responsibility, and visual gray image at last, which course can be called the second stage of the IRST. The first stage is related with the target distance, while the second stage is decided by the responding function itself of IRST.

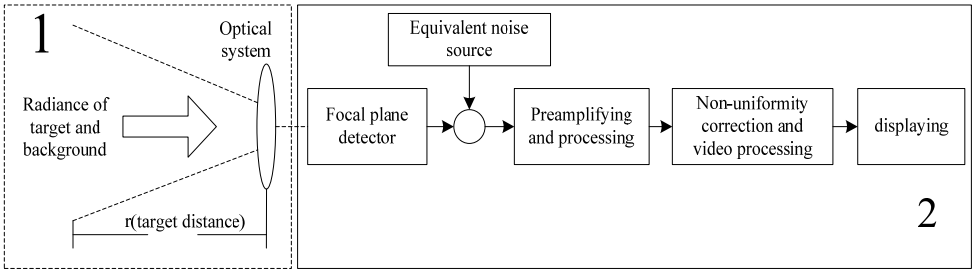

Fig. 1. The sketch map of IRST composition

At the first stage, the main influence factor is the atmosphere transmission ratio $\tau(\lambda, R) = e^{-\mu R}$, it contains an absorption coefficient $\mu = 4\pi\mu_e / \lambda$. Here the μ_e is the extinction coefficient. At the second stage, the radiant power is changed into voltage, and sampled as image gray, which course can be described by the relationship between the radiance and image gray approximately as

$$L = aG + L_{off} \tag{1}$$

Where L_{off} is the bias (constant) of target radiance, a is a constant related with the radiance and the pixel gray.

3. The relationship between IR pixel gray and radiance

As we usually adopted a two-dimensional staring focal plane array in infrared imaging system, which include N × M detection cells arranged as a matrix with N rows and M columns. After correction, each detection cell in the array has same IFOV, plus and bias. As the ultimate output of imaging system is image pixel, the correction is aimed to the relationship between the radiance $L(i)$ and the pixel gray $G(i)$ (where "i" means the grade number of the pixel gray). The expression is shown as

$$L(i) = aG(i) + L_{off} \tag{2}$$

If these parameters L_{off} and a are known accurately, then we can get the radiance of the target through the image pixel gray. We can get above two parameters by calibration data of the blackbody source.

For the blackbody source, the radiance reached the sensor can be expressed as follows, the surface radiant temperature of the blackbody source is recorded as T (K)

$$L_b = \int_{\lambda 0} \left\{ \tau_a(\lambda, r) \varepsilon M(\lambda, r) + \left[1 - \tau_a(\lambda, r) \right] M(\lambda, T_a) \right\} R(\lambda) d\lambda \tag{3}$$

Here, $M(\lambda, T)$ is the blackbody source emittance, ε is the emissivity of the blackbody source. $R(\lambda)$ is the relative spectral response of the system, with a assumption that $R(\lambda)$ is a constant. λ is the wavelength. r is the target distance. $\tau_a(\lambda, r)$ is absorption coefficient of the atmosphere. T_a is temperature of the atmosphere. As the target is 1.13 meter away with the sensor, the atmospheric attenuation can be ignored. And it is regarded as surface target, so the radiance is shown as

$$L_b = \int_{\lambda 0} \varepsilon M(\lambda, T) d\lambda \tag{4}$$

As the IR sensors are in a special band, such as 3-5um and 8-12um, the radiance can be explained as [12]

$$L_b = \int_{\lambda 1}^{\lambda 2} \varepsilon M(\lambda, T) d\lambda = F_{\lambda 1 - \lambda 2} \cdot \varepsilon \sigma T_b^4 \tag{5}$$

Here $F_{\lambda 1 \sim \lambda 2}$ denotes the ratio between the radiance of the given waveband with wavelength $\lambda 1 \sim \lambda 2$ and the one of the whole band. This can be gotten by the datasheet [13]. σ is the Stefan-Boltzmann constant, T_b is temperature of the blackbody source.

4. The blackbody source calibration test

The infrared sensors used here were cooled LWIR and MWIR sensors, they are all made in France corporation CEDIP, and the types are Jade 3 LW and Jade 3 MW F/2, and the detail technological index are shown as table 1.

sensor	Jade 3 LW	Jade 3 MW F/2
focus	50mm	50mm
NETD(25°C)	20mK	14.93mK
Noise	2.46DL	4.97DL
Sensitivity(25-26°C)	8.13mK/DL	3.01mK/DL
Image size(H×V)	320×240	320×240
Sample digit	14bit	14bit
Transmissivity of the optical system	>90%	>90%
Integral time	20, 50, 100, 200 microsecond	500, 1000, 2000, 2500 microsecond
Frame frequency	1-130Hz	1-130Hz
FOV	10.8°×8.1°	10.8°×8.1°
Spatial resolution	0.5mrad	0.5mrad
Size of image cell	25 μm ×25 μm	25 μm ×25 μm

Table 1. The technological index of LW and MW sensors

In the blackbody source calibration test, we use three blackbody source to calibrate the MW(3-5 μm)and LW(8-12 μm) staring sensors based on the GJB3756-99 criterion. And the result showed as the follow table.

	Blackbody source 1	Blackbody source 2	Blackbody source 3
Serial number	#163	#G0406011	#4845
Type	Plane	cavitary	cavitary
The range of temperature	0℃-100℃	100℃-950℃	100℃-1300℃
Uniformity of the radiant surface temperature/K	0.09	0.3	0.24(500℃)
Stability of temperature(K/h)	1.8	0.1	0.15(800℃)

Table 2. The index contrast of three blackbody sources

In the blackbody source calibration test, temperature of the blackbody source is known, so the relationship between $G(i)$ and $L(i)$ can be calculated. In this test, the two sensors are MW (3-5 um) and LM (8-12 um) staring infrared sensor, there integration time are 2500 and 200 us respectively; the blackbody source is a surface source and its temperature is adjustable from 5℃ to 100 ℃; the environmental temperature is 24 ℃; the relative humidity is 50 %. Fig.2 shows IR images of the blackbody source in 30 ℃ and 40 ℃ respectively:

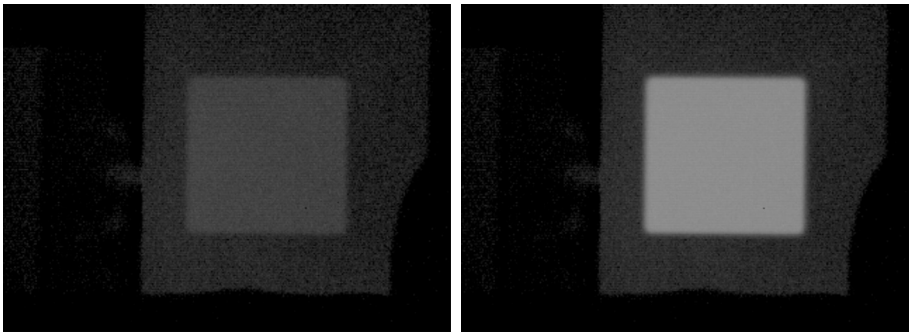

Fig. 2. MW IR image of blackbody source at 30℃and 40℃ respectively

Table3 shows the gray and temperature of the blackbody source counted by the MW and LW IR images.

	30℃	40℃
Gray of blackbody source in MW band	4333.18	5770.74
Gray variance of blackbody source in MW band	72.81	73.17
Gray of blackbody source in LW band	10257.67	11487.59
Gray variance of blackbody source in LW band	13.59	14.25

Table 3. The gray and gray variance of the target region

Therefore, based on equation (5), L_{off} and a can be counted as follows:

$$a_m = 0.0018;\ a_l = 0.0156; \tag{6}$$

$$L_{Moff} = \text{-}1.7908;\ L_{Loff} = \text{-}33.5507; \tag{7}$$

Here a_m and a_l denoted the variation ratio of MW and LM respectively, L_{Moff} and L_{Loff} denoted the radiance bias of MW and LW respectively.

After the blackbody source calibration, we can get the relationship between the target radiance, temperature and image gray, so we can use the outfield infrared images to analyze the infrared characteristic of the target.

5. Passive ranging based on single-band IRST

5.1 Radiance difference between point target and its background

When a target is quite far away from the IRST, the target image can not fill in the full detector elements, and the target can be treated as a point target[11], which is difficult to be ranged when a target is actionless as there is no shape, size etc. characteristics. Thus a target can only be ranged by using radiant and movement characteristics. At this scene, target, background and path radiance can arrive at the detector elements. The whole radiance of target and background is defined as

$$E_t = \left(I_t + L_b\left(\Omega_s - \Omega_t\right)\right)\tau\left(R_1\right)/R_1^2 + \left(1 - \tau\left(R_1\right)\right)L_a \tag{8}$$

For IR detection system, the whole radiance of target and background received by the detector is

$$L_t = \frac{E_t}{F} = \left[\left(I_t + L_b\left(\Omega_s - \Omega_t\right)\right)\tau\left(R_1\right)/R_1^2 + \left(1 - \tau\left(R_1\right)\right)L_a\right]/F \tag{9}$$

where I_t is the target whole radiant power, L_b is the background radiance, L_a denotes the atmosphere path radiance, $\tau\left(R_1\right)$ denotes the average atmosphere transmission on the transmitting path within the waveband of the detector, R_1 is the distance of a target and IRST, F is IFOV of the system, Ω_s is instantaneous scene, Ω_t is the angle between the target and the detector plane. When there is no target, the background will fill in the whole detector elements, and the received radiance is

$$L_b = \left[L_b\Omega_s\tau\left(R_1\right)/R_1^2 + \left(1 - \tau\left(R_1\right)\right)L_a\right]/F \tag{10}$$

Thus the radiance difference will be

$$\Delta L_1 = L_t - L_b = \left(I_t - L_b\Omega_t\right)\tau\left(R_1\right)/FR_1^2 \tag{11}$$

5.2 Radiance difference between surface target and background

For surface target, instantaneous scene Ω_s is smaller than angle Ω_t, thus the target image will take up several or even tens of detector elements as shown in Fig.3. Therefore the

surface target image includes target edge pixels and interior pixels. These edge pixels may reflect target, background and path radiance, while interior pixels may be only related with target and path radiance.

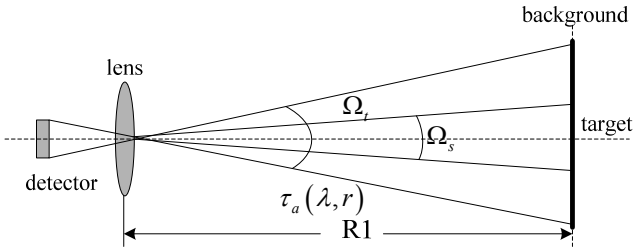

Fig. 3. The sketch map of the IR surface target's radiation

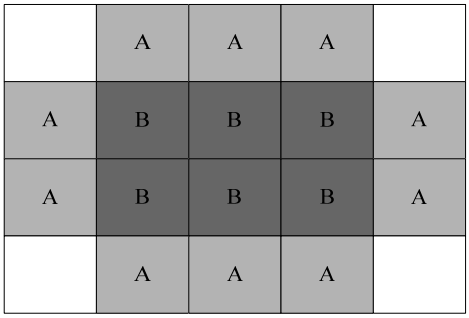

Fig. 4. The sketch map of the IR surface target

As Fig.4 depicts, surface target image includes inner pixels (denoted by "B") and edge pixels (denoted by "A"). Assuming an IR image produced by the staring IRST has N inner pixels and M edge pixels. For inner pixels, as the target is full to the detector elements, background radiance can not arrive at the detector, thus Ω_s equals to Ω_t, and the received radiance is, which is only decided by the target. For edge pixels, background radiance can arrive at the IR detector as the target is not full with the instantaneous scene. Assuming the IR radiance is L_{tB}, which reflects the sum of target and background radiance. For simplifying, we further assume that the background radiance is uniform distributed, and angles of target edge to the detector centre are all equal, we thus have

$$L_{tz}\ \ L_{tZ} = \sum_{i=1}^{N}\left[\left(L_{ti}\Omega_s / R_1^2\right)\tau\left(R_1\right) + \left(1-\tau\left(R_1\right)\right)L_a\right] \Big/ F \tag{12}$$

$$L_{tB} = \sum_{i=1}^{M}\left[\left(L_{ti}\Omega_{ti} + L_b\left(\Omega_s - \Omega_{ti}\right)\right)\tau\left(R_1\right) / R_1^2 + \left(1-\tau\left(R_1\right)\right)L_a\right] \Big/ F \tag{13}$$

Where L is the sum of target and background radiance, thus $L = L_{tZ} + L_{tB}$, and the target whole radiance power is I_t, besides

$$I_t = \sum_{i=1}^{M} L_{ti}\Omega_{ti} + \sum_{i=1}^{N} L_{ti}\Omega_s \tag{14}$$

Thus

$$L = \left[\left(I_t + \sum_{i=1}^{M} L_b\left(\Omega_s - \Omega_{ti}\right)\right)\tau\left(R_1\right)\Big/R_1^2 + \sum_{i=1}^{N+M}\left(1-\tau\left(R_1\right)\right)L_a\right]\Big/F \tag{15}$$

Where the radiance in the position of target corresponding pixel is L_{ti}, Ω_{ti} denotes the angle between target parts and detector element. A_t stands for the target area. When the target does not exist, the corresponding elements are filled with background radiance, defined as L where

$$L^{'} = \sum_{i=1}^{N+M}\left[L_b\Omega_s\tau\left(R_1\right)/R_1^2 + \left(1-\tau\left(R_1\right)\right)L_a\right]\Big/F \tag{16}$$

Therefore, the radiance difference ΔL of target and background is

$$\begin{aligned}\Delta L &= L - L^{'}\\ &= \frac{1}{FR_1^2}\left[I_t - L_b\left(\sum_{i=1}^{N}\Omega_s + \sum_{i=1}^{M}\Omega_{ti}\right)\right]\tau\left(R_1\right)\\ &= \frac{1}{FR_1^2}\left[I_t - L_bA_t\right]\tau\left(R_1\right)\end{aligned} \tag{17}$$

Comparing with the radiance difference computation for point and surface target, the two are the same and can use a same ranging method to obtain the distance, while target area A_t reflects their difference, which is more important to surface target.

5.3 Passive ranging for the airborne target with single waveband

Let the IRST be sustained in a ranging course, that there is no necessary for movement compensation for IR image. We thus take three targets measuring for target ranging. Set the IR image be $f_i(i=1\cdots3)$, and the interval between two measuring is same to ΔT. According to (1), the corresponding ΔL_i of the three images can be yielded from f_i as

$$\Delta L_i = a\left[G_t - G_B\right], i = 1,2,3 \tag{18}$$

Where the total gray of the target whole pixels is G_t, G_B denotes the total gray of the whole pixels when there is no target. Here the image gray of the background is set to the surroundings' for the no reiteration property of IR image. As the measuring intervals are quite short, we thus hold that the target area of each image is near equal to each other. According to (17), we can obtain that

$$\begin{cases}\xi_1 = \dfrac{\Delta L_1}{\Delta L_2} = \left(\dfrac{R_2}{R_1}\right)^2 e^{-\mu\left(R_1-R_2\right)}\\ \xi_2 = \dfrac{\Delta L_3}{\Delta L_2} = \left(\dfrac{R_2}{R_3}\right)^2 e^{-\mu\left(R_3-R_2\right)}\end{cases} \tag{19}$$

As the intervals of the three frame image are very short, we hold that the target move equably in this course, thus the distance difference for two near measuring is equal to ΔR, that is $R_2 - R_1 = R_3 - R_2 = \Delta R$, we can then obtain

$$\begin{cases} \xi_1 = \left(\dfrac{R_2}{R_2 + \Delta R} \right)^2 e^{-\mu \Delta R} \\ \xi_2 = \left(\dfrac{R_2}{R_2 - \Delta R} \right)^2 e^{\mu \Delta R} \end{cases} \tag{20}$$

From which the target distance R_2 and ΔR can be obtained.

5.4 Experiment results and error analysis

Experiment data is produced by long and medium wave staring IR sensors at pm in Oct.18 of year 2006. The air temperature is 15℃ and it is sunshine. Civil aero-plane is used. The image format is 320×240. The atmosphere long wave attenuation coefficient is 2.17, while it is 1.45 in medium wave situation according to the Lowtran software. Fig.5 presents the IR images for both point target and surface target. The target distance is obtained by GPS and radar in the experiments.

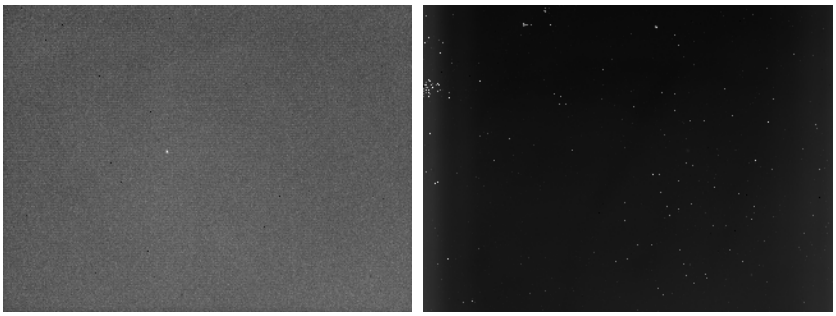

Point target(medium wave) Point target(long wave)

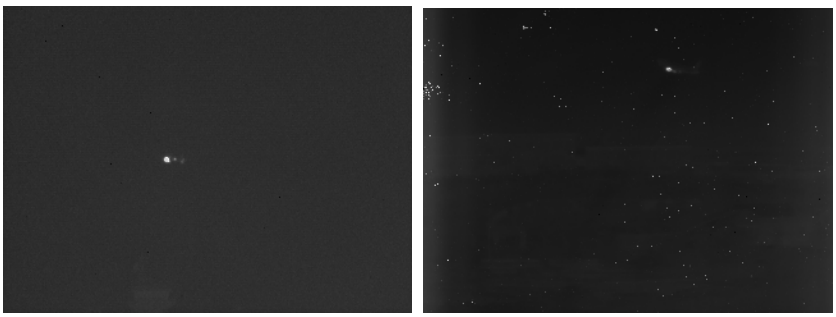

Surface target(medium wave) Surface target(long wave)

Fig. 5. The two MW/LW IR outfield images

For point target, we can achieve the gray difference between target and background, making use of the gray of surroundings as the gray of background. But for surface target, compute the total pixels and the total gray of surface target when dividing surface target from image firstly, and then compute the total gray of background when replacing the gray of target with surrounding'. We achieve the gray difference between surface target and background accordingly.

As the pivotal factor, different division thresholds result in the quantitatively difference of target pixels.

Experiment data is chosen from the image data when the plane is in the climbing phase. We choose 3 frames of image data per second, which has the equal space between frames, which is 240ms. Based on the algorithm provided in the paper, the distance of one target is achieved. The total experiment time is 10 seconds. Fig.6 present the distance comparison of surface target, which is counted by IR data of actual measurement in a period of time, and by the radar data.

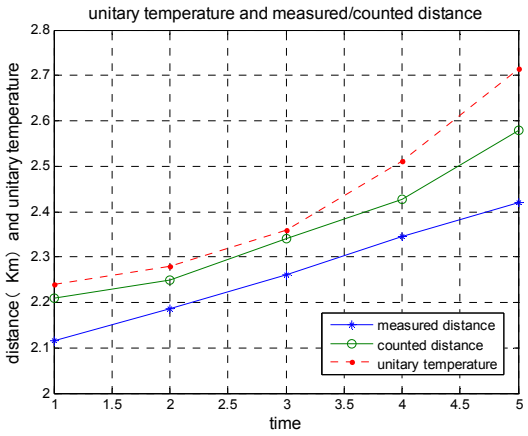

Fig. 6. Counted distance (LW/MW) and measured distance of surface target

The distance comparison of point target is shown in Fig.7, which contain the distance counted by the IR image of actual measurement in a period of time, the distance difference between frames, and the distance measured by radar. Restricted by the functionary distance of IR sensors, experiment time is only 5 seconds.

Hereinafter, the experiment results are analyzed:

1. For the actual experiment, the algorithm provided in the paper has a fixed error. The reason is that, the target is moving at a constant velocity in the hypothesis of this paper, but the phase of target climbing is an accelerated phase. Method of reduce error is reducing the gap between frames.
2. The target distance counted by long wave IR data is more accurate than which counted by medium wave data. The main reason is that, the functionary distance of long wave IR sensor is farer, and the contrast and the contour of target is clearer, which is propitious to acquire more accurate radiance difference between target and background, as to long wave IR image. The algorithm provided in the paper need to count the total pixels of target.

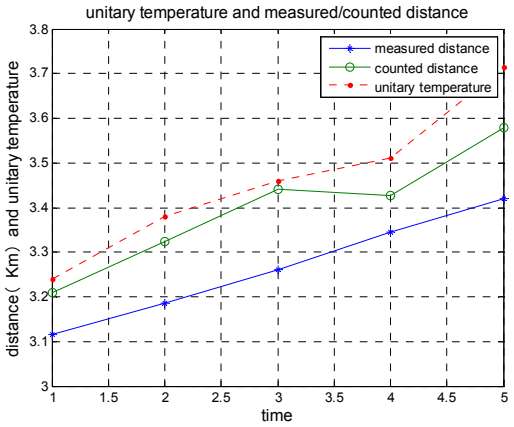

Fig. 7. Counted distance (LW/MW) and measured distance of point target

3. In the experiment, the results has a larger error counted at the time of 4 and 5, when target attitude has some change, that results in the change of target's contour. Consequently, the distance counted has some jitter. But for radar, the change of target attitude has little effect on distance in range.
4. The results of counted distance of surface target are better than point target's. And, for surface target, the farer distance of target, the larger error of results. When the target is farer, the area of target is smaller in image. For surface target, division threshold and the total pixels of target is less accurate, which results in worse result of radiance difference between target and background, further, affect distance measure. But for point target, the distance of target is counted by single pixels. If the gray of these pixels is inaccurate, there will be larger error of distance measure or ranging.
5. A great influence on the veracity of distance measure has the atmospheric attenuation coefficient. This paper uses a average coefficient of atmospheric attenuation, which introduces a fixed error, in spite of omitting the complicated integral.
6. The algorithm about passive ranging of single-band provided in the paper has the following hypotheses: one is that target is moving at a constant velocity in the short time among measures approximately; another is that the area of target is approximately constant in the period. Thus, the algorithm fits the passive ranging of air mobile target well, instead of ground mobile target.

The measure error is analyzed:

1. Influences of radiance of background

The expression of (10) is the computation of the radiance of background for surface target. Because of in the actual imaging, we achieve the average radiance of background approximately, using of the gray of background around the target, instead of computing according to (10) when the target is divided up. And then according to the total pixels of target, compute the whole radiance of background, in this way, which has a fixed error itself. When it is a surface target, the error is severe.

2. Influences of the atmospheric extinction coefficient

Another error is brought into ranging due to the atmospheric extinction coefficient, which contains the following two aspects: (1) The error is introduced when using the average atmospheric extinction coefficient to simplifying the integral. (2) The atmospheric extinction coefficient is computed by the Lowtran7 software. When the circumstance parameter is inaccurate, the atmospheric extinction coefficient will has error, results in the error of ranging.

3. Influence of target range

The farer is target range, the larger error is introduced. When the target is farer, the area of target is smaller in the image, accordingly, results in compute error in the difference of radiation power between target and background, thus, affects ranging. For point/surface target, the difference of radiance difference between target and background is presents, when R_m is the measure precision of range.

$$\Delta L = \frac{1}{FR_1^2}\left[I_t - L_b A_t\right]\tau\left(R_1\right) \tag{21}$$

When compute the derivative of R, we has

$$\frac{d\Delta L}{dR} = \frac{\left[I_t - L_b A_t\right]}{FR_1^2} e^{-\mu R}\left(-\mu - \frac{2}{R}\right) \tag{22}$$

$$dR = \frac{\left(d\Delta L\right) FR_1^2}{\left[I_t - L_b A_t\right] e^{-\mu R}\left(-\mu - 2/R\right)} \tag{23}$$

According to (17), when the farer the target range is, the worse the measure precision is; the smaller is the resolution of the pixel gray of IR image, the better is the measure precision.

6. Surface target ranging based on single-station dual-band IRST

The algorithm above is also applicable for multiband, with a presupposition of point or tiny targets. When there are surface targets, the estimation of background radiance brings severe error, which causes the algorithm invalid. Therefore, another range measurement algorithm for surface targets is proposed in the next section.

6.1 Calculation of surface target radiance

When the target is far from the infrared detector, it can be regarded as a point target [11]. There is not only the target radiation but also the background and path radiation can reach the detector cell. So the radiance flux of the detector cell is：

$$E_t = F(r)\int_{\lambda_0}\left\{\tau_a\left[\varepsilon_t M\left(\lambda, T_t\right) + \rho_l M\left(\lambda, T_{ae}\right)\right] + \left[1 - \tau_a\right] M\left(\lambda, T_a\right)\right\} d\lambda \tag{24}$$

In above formula, $\varepsilon_t + \rho_l = 1$, ε_t is the target emissivity, ρ_l is the target reflectivity. $F(r)$ is geometrical factor related with the target distance r. $M(\lambda, T_t)$ is the radiation flux density of the target region; $M(\lambda, T_{ae})$ is the background radiation flux density reflected by the background; $M(\lambda, T_a)$ is the radiation flux density reflected by the atmospheric path ; τ_a is the transmission ratio of the light path between the infrared detectors and the target; T_t is the temperature (K) of the target; T_a is the atmospheric temperature (K).

When the military targets (such as aircraft) near the detector, the goal may occupy several even dozens of detector cells, so it is more appropriately to regard them as surface targets. As shown in Fig.3, Ω_s (the instantaneous field of view of the detector) is smaller than Ω_t (the target stretching angle relative to the detector cell), so both target and background radiation can reach the fringe detection cell, but only the target and path radiation can reach the internal detection cell. Because the edge pixels are fewer than the internal pixels, the paper takes the internal pixels into count mainly.

According to the internal pixels, the target area fills instantaneous field of view (IFOV) of the sensor completely, $F(r)$ is IFOV of the system, it is Ω_s. The radiance of the target reached the sensor is:

$$L_t = E_t / F(r) = E_t / \Omega_s \tag{25}$$

$$L_t = \int_{\lambda_0} \left\{ \tau_a \left[\varepsilon_t M(\lambda, T_t) + \rho_l M(\lambda, T_{ae}) \right] + \left[1 - \tau_a \right] M(\lambda, T_a) \right\} d\lambda \tag{26}$$

In appointed band, the radiance can be described as

$$L_t = \int_{\lambda 1}^{\lambda 2} \left\{ \tau_a \left[\varepsilon_t M(\lambda, T_t) + \rho_l M(\lambda, T_{ae}) \right] + \left[1 - \tau_a \right] M(\lambda, T_a) \right\} d\lambda \tag{27}$$

Here the integral process can be describe as

$$L_t = F_{\lambda 1 \sim \lambda 2} \tau_a \varepsilon_t \sigma T_t^4 + F_{\lambda 1 \sim \lambda 2} \sigma T_{ae}^4 \left[\tau_a \rho_l + 1 - \tau_a \right] \tag{28}$$

In above expression, $F_{\lambda 1 \sim \lambda 2}$ denotes the ratio between the radiance of the given waveband with wavelength $\lambda 1 \sim \lambda 2$ and the one of the whole band. T_t is the target temperature, T_{ae} is the atmosphere temperature. As $\varepsilon_t + \rho_l = 1$, we can get following equation

$$L_t = F_{\lambda 1 \sim \lambda 2} \sigma T_{ae}^4 + F_{\lambda 1 \sim \lambda 2} e^{-\mu R} \varepsilon_t \sigma \left(T_t^4 - T_{ae}^4 \right) \tag{29}$$

6.2 Passive ranging based on the single-station dual-band infrared images

Based on the equation (2) we can get the target radiance from the image pixel gray. In the above equation, the $F_{\lambda 1 \sim \lambda 2}$, T_{ae} and ε_t are known. The target temperature T_t is known roughly, and the target distance R is unknown totally.

As there are dual-band infrared sensors on the same platform. At the same time we can get two frames infrared image, they all aim at the same target area. According to expression (29) we can obtain the radiance of the same target area at different band.

Assume A means the same target area in the two infrared images; its temperature and distance should be equal approximately according to different band, recorded as T_A (known roughly) and r_A (unknown). We can get its radiance by LW and MW infrared image, recorded as L_M and L_L respectively. The atmospheric extinction coefficients in LW and MW bands were known as μ_M and μ_L respectively, so L_M and L_L can be expressed as follows:

$$L_M = F_{\lambda 1 \sim \lambda 2}\sigma T_{ae}^4 + F_{\lambda 1 \sim \lambda 2} e^{-\mu_M R}\varepsilon_t \sigma\left(T_t^4 - T_{ae}^4\right) \tag{30}$$

$$L_L = F_{\lambda 1 \sim \lambda 2}\sigma T_{ae}^4 + F_{\lambda 1 \sim \lambda 2} e^{-\mu_L R}\varepsilon_t \sigma\left(T_t^4 - T_{ae}^4\right) \tag{31}$$

So we use the iteration method to get the T_t and R from the above two equations.

There will be much error if we adopt only one pixel of the target in infrared image, so we must use a few pixels of the target at the same time.

Firstly after image matching, the two infrared images are aimed to the same scene; then the target is segmented and a few pixels are chose at the same position of the two images. Secondly the radiance L_i according to each target pixel can be calculated by each pixel gray G_i. Thirdly the target distance r_i can be counted by the dual-band radiance of the pixels. Lastly the distance deduced by different target pixels should be chosen in reason and their average value will be used as the ultimate distance.

The algorithm is shown as follows

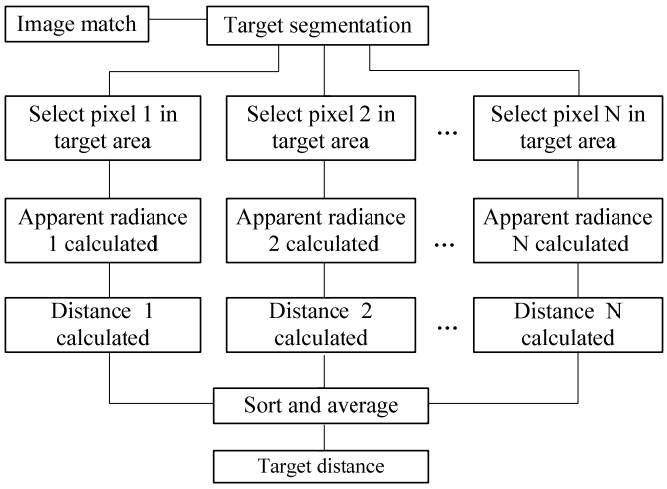

Fig. 8. The ranging process of surface target

6.3 Experiment results and error analysis

Experiments have been done to verify the ranging algorithm in October, the air temperature was 15 ℃, the target was aircraft, FOV(Field Of-View) and IFOV(Instantaneous Field Of-View) of the two sensors were same as 10.8o × 8.1o and 0.5 mrad. Fig.9 show the LW and MW IR image at the same time, and the bright point was the aircraft.

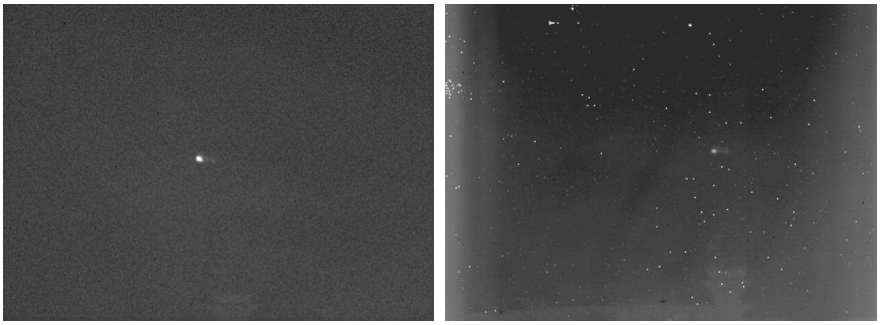

Fig. 9. MW and LW infrared images of the aircraft

Table4 shows the target distance, a certain pixel gray and temperature of the same target at six different times (time interval is about one second).

Time	Pixel gray in MW band	Pixel gray in LW band	Calculated distance (Km)	Measured distance by radar(Km)	Target temperature (K)
0	16087	11230	0.9949	0.885	387.95
1	15868	11149	0.985	0.948	387.11
2	15715	11070	0.958	1.004	386.66
3	15241	10802	1.101	1.060	386.48
4	15278	10648	1.159	1.116	386.86
5	15752	10508	1.239	1.172	391.04

Table 4. Distance, temperature and metrical distance at different moments

Fig.10 is gained by above table, and we can get the movement trends of the target from the figure intuitionally. The figure shows the unitary value of measured distance, calculated distance and temperature.

Test results and analysis:

1. From time2 to time5, the average error between measurement and calculation is less. The reason is that the radar ranging is based on radar scattering centres of the target, and the infrared ranging is based on the surface of the target, there will be errors unavoidably.
2. The errors at time 0 is remarkable because that the distance is very close at each moment, the target pixels have reached a saturation level according to the integration time of the infrared sensor, so the ranging is not accurate.

3. With the distance become more and more farer, the target get smaller and smaller in the IR image. The target has become increasingly unclear according to the same sensor integration time (relative to above moment), it is very difficult to find a same pixel in two infrared images, so it will also have a greater error.
4. The target temperature is equal approximately in fig.10. In fact, as it is the same target, the temperature won't have much change when the target distance is not half far enough.

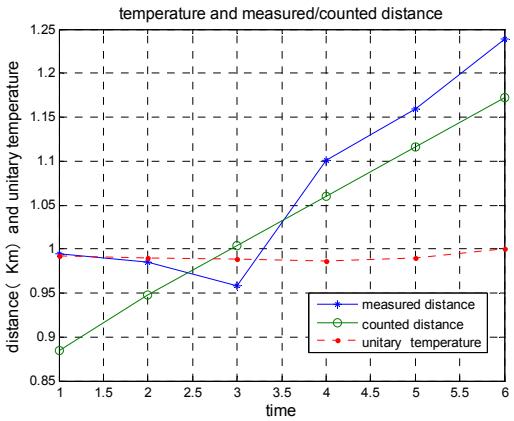

Fig. 10. Measured and calculated distance at five times

The above error is related with the sensor integration time. The paper will analyze the algorithm and find which factors will be likely to bring ranging error.

1. Will the inaccurate atmospheric extinction coefficient bring the ranging error?

From the equation 17 we can know that the error of atmospheric extinction coefficient will bring the ranging error.The error mainly includes the following two aspects: (1) the paper uses the average atmospheric extinction coefficient to simplify the integration process, it will bring ranging error. (2) The atmospheric extinction coefficient is calculated by LOWTRAN7 software in this paper, inaccurate environmental parameters will lead to inaccurate calculation, and therefore it will cause the ranging error.

2. Will the mismatch of pixels bring the ranging error?

If the chosen pixels are not in the same position of a target, their range and radiance is different, so it will bring errors in ranging process.

As the ground environment is more complex than the air environment, the algorithm has only used in airborne ground targets ranging; the author will do more tests to carry out ground targets ranging.

7. Conclusion

This paper regarded passive ranging based on IR radiation characteristics as researching background. The operating principle of staring IRST was analyzed. Then the relationship

between IR pixel gray and radiance was deduced. And the parameters were got through the blackbody source calibration test. In the single-band and dual-band situations, according to point and surface target, we deduced two ranging methods respectively. Lastly the algorithm was validated for point and surface target by outfield IR image, the ranging error was analyzed also.

8. Acknowledgment

Here, I sincerely thank Dr. Vasyl Morozhenko pointed out the inadequacies in my paper.

9. References

[1] Wang Gang, Yu Bin-Xi. Approach to estimate infrared point-target detection range against sky background based on contrast. Optics and Precision Engineering, Vol.10 No.3, Jun.2002, pp276-280.

[2] Xing Qiang, Huang Hui–ming, Xiong Ren-sheng, Yu Tao. Detect ability Analyzing of IR FPA Tracking System. ACTA PHOTOICAS INICA, Vol.33 No.7, July.2004, pp894-897.

[3] Yin Shi-min, Fu Xiao-ning, Liu Shang-qian. Research for Infrared Mono-station Passive Location on Stationary Platform. ACTA PHOTOICAS INICA, Vol.33 No.2, Feb.2004, pp237-239.

[4] Lu Yuan, Ling Yong-shun, Wu Han-ping, Li Xiao-xia. Study on Passive Distance Measurement of Ground Objects by Infrared Radiation. J.Infrared Millim.Waves, Vol.23 No.1, Feb.2004, pp77-80.

[5] Lu Yuan, Ling Yong-shun, Shi Jia-ming. Measurement of Aerial Point Target Distance Using Dual-band Infrared Imaging System. Optics and Precision Engineering, Vol.12 No.2, Apr.2004, pp161-164.

[6] Feng Guo-qiang, Zou Qiang, Li Wei-ren. Algorithm of Passive Ranging by Single Station. Infrared Technology, Vol.27 No.4, July.2005, pp295-298.

[7] Anders G.M. Dahlberg, Olof Holmgren. Range performance modeling for staring focal plane array infrared detectors. Infrared Imaging Systems: Design, Analysis, Modeling, and Testing XVI, Proceedings of SPIE, 2005, Vol.5784, pp81-90.

[8] Wang Bing-xue, Zhang Qi-heng, Chen Chang-bin, Wang Jing-ru, He Xue-mei. A Mathematical Model for Operating Range of A Staring IR Search and Track System. Opto. Electronic Engineering, Vol.31, No.7, July.2004, pp8-11.

[9] Wang Wei-hua, Niu Zhao-dong, Chen Zeng-ping. Research on The Operating Range of Staring IR Imaging System in Sea-Sky Background. J.Infrared Millim.Waves, Vol.25, No.2, Apr.2006, pp150-153.

[10] Bai Yan-zhu, Jin Wei-qi. Principle and Technology of Optical-Electronic Imaging. Beijing Institute of Technology Press.

[11] Pieter A. Jacobs Write, Wu Wen-jiann, Hu Bi-ru, Man Ya-hui Translate. Thermal Infrared Characterization of Ground Targets and Backgrounds. National Defense Industry Press. 2004.

[12] Richard D. Hudson, JR. Infrared System Engineering. John Wiley & Sons, INC. 1969.

[13] Yang Chen-hua, Mei Shui-sheng, Lin Jun-ting. Laser and Infrared Technological Datasheet. National Defense Industry Press. 1990.

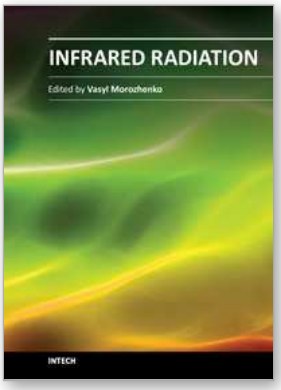

Infrared Radiation

Edited by Dr. Vasyl Morozhenko

ISBN 978-953-51-0060-7
Hard cover, 214 pages
Publisher InTech
Published online 10, February, 2012
Published in print edition February, 2012

This book represents a collection of scientific articles covering the field of infrared radiation. It offers extensive information about current scientific research and engineering developments in this area. Each chapter has been thoroughly revised and each represents significant contribution to the scientific community interested in this matter. Developers of infrared technique, technicians using infrared equipment and scientist that have interest in infrared radiation and its interaction with medium will comprise the main readership as they search for current studies on the use of infrared radiation. Moreover this book can be useful to students and postgraduates with appropriate specialty and also for multifunctional workers.

INTECH
open science | open minds

InTech Europe
University Campus STeP Ri
Slavka Krautzeka 83/A
51000 Rijeka, Croatia
Phone: +385 (51) 770 447
Fax: +385 (51) 686 166
www.intechopen.com

InTech China
Unit 405, Office Block, Hotel Equatorial Shanghai
No.65, Yan An Road (West), Shanghai, 200040, China
中国上海市延安西路65号上海国际贵都大饭店办公楼405单元
Phone: +86-21-62489820
Fax: +86-21-62489821